

Inelastic neutron scattering study of hydrogen in d_8 -THF/D₂O ice clathrate

Kimberly T. Tait,^{a)} Frans Trouw,^{b)} and Yusheng Zhao

Manuel Lujan Jr. Neutron Scattering Center, Los Alamos National Laboratory, Los Alamos, New Mexico 87545, USA

Craig M. Brown

Indiana University Cyclotron Facility, Indiana University, Bloomington, Indiana 47408, USA and National Institute of Standards and Technology, Center for Neutron Research, Gaithersburg, Maryland 20899, USA

Robert T. Downs

Department of Geosciences, University of Arizona, Tucson, Arizona 85721, USA

(Received 22 February 2007; accepted 2 August 2007; published online 5 October 2007)

In situ neutron inelastic scattering experiments on hydrogen adsorbed into a fully deuterated tetrahydrofuran-water ice clathrate show that the adsorbed hydrogen has three rotational excitations (transitions between $J=0$ and 1 states) at approximately 14 meV in both energy gain and loss. These transitions could be unequivocally assigned since there was residual orthohydrogen at low temperatures (slow conversion to the ground state) resulting in an observable $J=1 \rightarrow 0$ transition at 5 K ($kT=0.48$ meV). A doublet in neutron energy loss at approximately 28.5 meV is interpreted as $J=1 \rightarrow 2$ transitions. In addition to the transitions between rotational states, there are a series of peaks that arise from transitions between center-of-mass translational quantum states of the confined hydrogen molecule. A band at approximately 9 meV can be unequivocally interpreted as a transition between translational states, while broad features at 20, 25, 35, and 50–60 meV are also interpreted to as transitions between translational quantum states. A detailed comparison is made with a recent five-dimensional quantum treatment of hydrogen in the smaller dodecahedral cage in the SII ice-clathrate structure. Although there is broad agreement regarding the features such as the splitting of the $J=1$ degeneracy, the magnitude of the external potential is overestimated. The numerous transitions between translational states predicted by this model are in poor agreement with the experimental data. Comparisons are also made with three simple exactly solved models, namely, a particle in a box, a particle in a sphere, and a particle on the surface of a sphere. Again, there are too many predicted features by the first two models, but there is reasonable agreement with the particle on a sphere model. This is consistent with published quantum chemistry results for hydrogen in the dodecahedral 5^{12} cage, where the center of the cage is found to be energetically unfavorable, resulting in a shell-like confinement for the hydrogen molecule wave function. These results demonstrate that translational quantum effects are very significant and a classical treatment of the hydrogen molecule dynamics is inappropriate under such conditions. © 2007 American Institute of Physics. [DOI: 10.1063/1.2775927]

I. INTRODUCTION

Understanding the mechanism of hydrogen adsorption into novel materials is of considerable interest from the perspective of hydrogen storage for a future hydrogen fuel economy. The discovery of hydrogen-water ice clathrate¹ demonstrated that at high pressures (200 MPa) hydrogen can act as a templating agent for clathrate formation. A subsequent study² showed that a ternary clathrate could be formed between hydrogen, tetrahydrofuran (THF), and water at a much reduced hydrogen gas pressure. This reduction in pressure is attractive from an engineering perspective for hydrogen storage applications.

There has been some ambiguity regarding the location

and quantity of hydrogen adsorbed in THF clathrate. The large cages are all filled by the THF, and so the hydrogen is expected to reside in the smaller dodecahedral (5^{12}) cavity. Mao *et al.*¹ indicated that the small cage contains two hydrogen molecules in the pure hydrogen clathrate, though this conclusion has been the subject of some controversy, and a recent study reported by Hester *et al.*³ using neutron diffraction concluded that there is only single occupancy of the small cage in THF-ice clathrate.

Neutron spectroscopy has been extensively used to characterize the dynamics of hydrogen adsorbed in a wide variety of materials, such as alkali metal graphite intercalation compounds,⁴ zeolites,⁵ and in the octahedral interstitial sites in solid C₆₀.⁶ At low temperatures, it is straightforward to measure the quantum rotor states and center-of-mass modes of the hydrogen molecule, while quasielastic scattering occurs when there is diffusive rotational or translational mo-

^{a)}Now at Department of Natural History, Royal Ontario Museum, Toronto, Ontario M5S 2C6, Canada. Electronic mail: ktait@rom.on.ca

^{b)}Electronic mail: trouw@lanl.gov

tion. Hydrogen has a relatively large neutron scattering cross section, and the relative contribution from the hydrogen can be further enhanced by deuterating other components.

This study uses inelastic neutron scattering to study the dynamics of hydrogen in the ternary clathrate formed between water, THF, and hydrogen. The results show that the quantum rotor states are only perturbed to a small extent upon adsorption, while the translational quantum states are significantly modified by confinement in the clathrate cage.

II. METHODS

Neutron inelastic scattering measurements were made on the Pharos spectrometer located at the Lujan Center, Los Alamos National Laboratory and on the disk chopper spectrometer⁷ (DCS) at the National Institute of Standards and Technology Center for Neutron Research (NCNR). These are complementary instruments as Pharos is designed for thermal neutron experiments using incident energies in the range of 15–1000 meV, while DCS uses cold neutrons (e.g., 3 meV) to attain a much better elastic energy resolution. The Pharos experiment therefore focused on relatively large neutron energy loss scattering, while the DCS was used to look for low energy excitations on the order of 1 meV and for evidence of quasielastic neutron scattering.

A. Pharos

The Pharos spectrometer is on a pulsed neutron source, viewing a room temperature water moderator. Certain commercial materials and equipment are identified in order to specify adequately experimental procedures. In no case does such identification imply recommendation or endorsement by the National Institute of Standards and Technology, nor does it imply that the items identified are necessarily the best available for the purpose. Perdeuterated THF (99.95% D, Aldrich) and D₂O (99.9% D, Aldrich) were mixed in the mole ratio of 1:17 and frozen to form a fully deuterated THF-ice clathrate. This was crushed using a mortar and pestle in a helium atmosphere, and then transferred to the aluminum scattering container. All of the equipment and the clathrate were kept cold using dry ice.

The aluminum sample container is a pressure vessel with eight parallel cylindrical channels of 5 mm in diameter cut into a flat piece of aluminum, with excess aluminum removed between the channels. The channels are connected via a common channel formed between the lid and the body of the cell. The lid has a connection to a capillary gas line for the application of gas pressure to the sample.

After filling, the cell was quickly mounted on the tip of a helium closed cycle refrigerator at approximately 250 K. This was then placed in the sample chamber and the chamber evacuated to at least 10⁻³ Pa. The sample container was then warmed to 265 K in order to remove any residual ice on the external surface of the sample container.

Hydrogen at a pressure of approximately 14 MPa was then applied to the THF-ice clathrate at 270 K. The sample was subsequently valved off from the hydrogen source and the pressure monitored to see if the pressure dropped due to incorporation of the hydrogen into the clathrate. This drop in

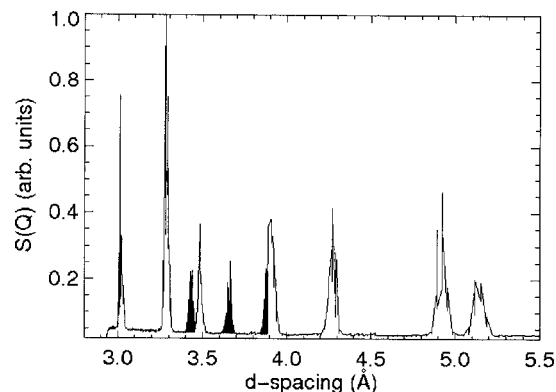


FIG. 1. Diffraction pattern from ternary clathrate H₂/d₈-THF/D₂O at 5 K measured on DCS with an incident wavelength of 5.5 Å. The three shaded peaks are from residual ice in the sample.

pressure was observed, but there was clearly also a small leak into the sample chamber and so the pressure drop data are ambiguous. The valve to the hydrogen bottle was periodically opened to maintain a hydrogen pressure greater than 10 MPa.

After several hours, the sample was cooled to 100 K while maintaining the hydrogen pressure at 14 MPa, and then the excess gaseous hydrogen was pumped off, assuming that all of the hydrogen in the clathrate was trapped at that temperature. The sample was further cooled to 8 K and the inelastic scattering measured using incident energies of 70, 40, 25, and 15 meV. Measurements were also carried out at temperatures of 50 and 100 K at a variety of incident energies ranging from 40 to 120 meV (Fermi chopper frequencies of 240 Hz at 40 and 70 meV and 360 Hz at 120 meV).

B. DCS

Preparation of a *d*-THF-D₂O sample was carried out in a similar manner and this was loaded into a cylindrical aluminum sample cell with a diameter of 12.7 mm and a sample bore of 10 mm. The sample cell was put into a standard liquid-helium cryostat and the scattering from the THF clathrate measured at 5, 50, 100, 150, and 200 K. Hydrogen was then added in a similar manner to the Pharos experiment and the excess gas pumped off at 100 K. Scattering measurements were then made at sample temperatures of 5, 50, 100, and 150 K. An incident wavelength of 5.5 Å was used, yielding an elastic energy resolution of 90 μeV full width at half maximum.

III. RESULTS

The experiments on the Pharos and DCS spectrometers yielded very similar results, which demonstrated the reproducibility of the sample preparation. Even with a monochromatic incident neutron beam, it was possible to measure a useful *in situ* diffraction pattern from the samples since both instruments have detectors covering a wide range of 2θ. An example of the diffraction patterns measured on DCS is shown in Fig. 1.

The diffraction pattern shows strong peaks from the clathrate, in addition to the characteristic triplet from water

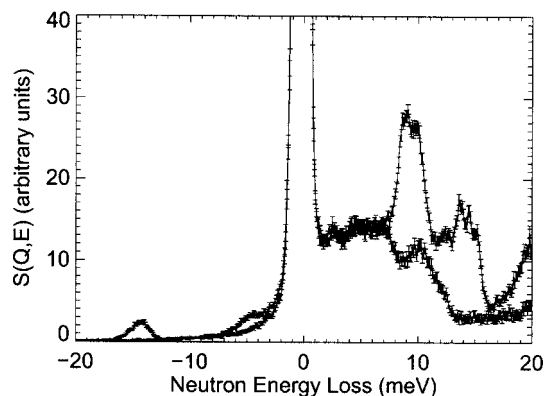


FIG. 2. Inelastic scattering spectra from THF-ice clathrate before and after the addition of hydrogen measured at 8 K on Pharos with an incident neutron energy of 40 meV.

ice in the range of 3.4–4 Å. Although some ice is present, it is a minor component of the sample and in any case not important from the perspective of this experiment as it will not absorb any hydrogen at 14 MPa.

The diffraction pattern from the ternary clathrate is expected to be very similar. Inspection of the neutron diffraction pattern for the fully filled D_2/d_8 -THF/ D_2O clathrate published by Hester *et al.*³ shows that the most visually resolved difference upon deuterium adsorption is the change in intensities in the two peaks around 2.75 Å. These cannot be seen in the diffraction pattern in Fig. 1, as the d -spacing cutoff for DCS operated with a wavelength of 5.5 Å is just above that at about 2.9 Å. It was also not possible to resolve this feature in the Pharos data since the instrument has poor resolution when operated in constant wavelength mode.

Figure 2 shows a comparison between the inelastic scattering spectra for the THF clathrate measured on Pharos before and after the addition of the hydrogen. There is extra scattering from the hydrogen on both the neutron energy gain and loss side, as is expected for a mix of para- and ortho-hydrogen. The two spectra were scaled by the integrated number of protons on the spallation target which is proportional to the total number of incident neutrons for each measurement.

Detailed analyses of the scattering from the hydrogen (THF-clathrate scattering has been subtracted) are shown in Figs. 3 and 4. On the neutron energy gain side, a model incorporating three Gaussians and a sloping background was fitted to the extra scattering, while a total of six Gaussians and a sloping background was fitted to the neutron energy loss data.

The resolution of the Pharos spectrometer was estimated using the MCSTAS Monte Carlo simulation code.⁸ All of the incident beam optics and known moderator performance were included in the estimate of instrument energy resolution. A single detector was chosen to evaluate the performance of the spectrometer, located at $2\theta=135^\circ$ with the flat sample at 45° to the incident beam direction. The predicted energy resolution was linear over the energy transfer range of interest, both for 70 and 40 meV incident neutron energies [full width at half maximum (FWHM)= $3.06-0.04\Delta E$ meV at 70 meV and FWHM= $1.47-0.04\Delta E$ meV at 40 meV].

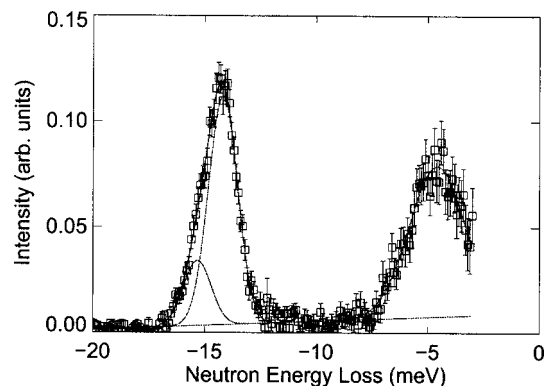


FIG. 3. Model fit using multiple Gaussians and a sloping background for the neutron energy gain data measured on Pharos at 8 K with a neutron incident energy of 40 meV, after subtraction of the bare clathrate signal. Individual components are shown, and the solid line through the points is the overall fit to the data.

The dominant effect on the energy resolution as a function of energy transfer was the broadening in time of the transmitted neutron pulse due to the range of velocities transmitted through the Fermi chopper (i.e., moderator pulse width).

There are discrepancies between the fitted widths of the peaks and those predicted by the instrument resolution simulation. This could be a consequence of the overlap of the multiple features, or possible a result of an inadequate pulse width model for the neutron moderator. Nevertheless, the locations of the most of the features are visually obvious, and the uncertainties will lie mainly in the width and intensity of the peaks.

Similar results were obtained on the DCS spectrometer, though this instrument is primarily designed to operate with cold neutrons and so the neutron energy loss range is typically reduced to a few meV. The neutron energy gain spectra for the ternary clathrate of 5 and 50 K are shown in Figs. 5 and 6. There is shift in intensity to a higher energy transfer shoulder at 50 K, which is consistent with an increased population of a higher energy state.

A good fit of these spectra required two Gaussians at 5 K and three Gaussians at 50 K (both fits include a sloping linear background). The positions of the Gaussians at 5 K are -13.58 ± 0.01 and -13.99 ± 0.03 meV, while at 50 K the cen-

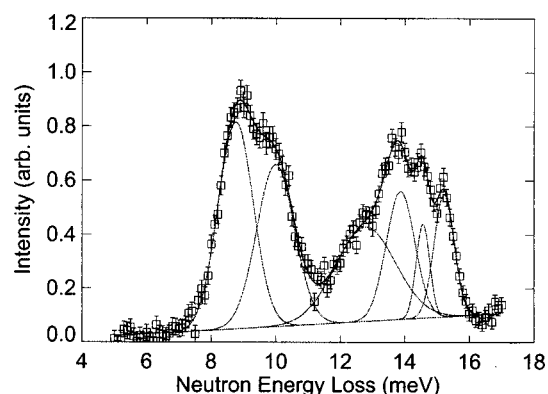


FIG. 4. Model fit using multiple Gaussians and a sloping background for the neutron energy loss data measured on Pharos at 8 K with a neutron incident energy of 40 meV. Individual components are shown, and the solid line through the points is the overall fit to the data.

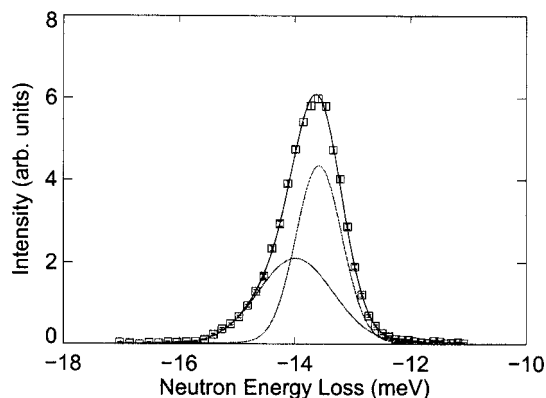


FIG. 5. Neutron energy gain peaks observed on DCS at 5 K fitted with two Gaussians. Individual components are shown, and the solid line through the points is the overall fit to the data.

ters are at -14.7 ± 5.05 , -13.72 ± 0.03 , and -5.54 ± 1.64 meV (last peak compensates for increased scattering at lower energies at 50 K). It is not possible to meaningfully resolve the individual features obtained on Pharos in neutron energy loss with an incident energy of 40 meV, but the increase in intensity on the higher energy side of the broad peak is consistent with an increased population of the higher energy rotational states at 15.22 and 14.57 meV.

There are additional higher energy features in the spectra from the ternary clathrate at 8 K on Pharos, which are not present in the THF-ice clathrate spectrum (Fig. 7). There are two sharp peaks next to each other at approximately 28 meV (27.44 ± 0.11 , 28.95 ± 0.07 meV) and some broader features at 20, 23, and 36 meV. The two sharper peaks show quite different Q dependence, with the higher energy excitation peaking in intensity before the lower energy peak.

IV. DISCUSSION

A. Rotational quantum states

It is not possible to assign four peaks to transitions between the $J=0$ and $J=1$ quantum states, as the $J=1$ state has a degeneracy ($2J+1$) of 3, and the ground state is singly degenerated. Possible explanations are (1) distinct types of hydrogen molecular adsorption sites; (2) transitions from the $J=1$ to a state approximately 12 meV higher in energy; or

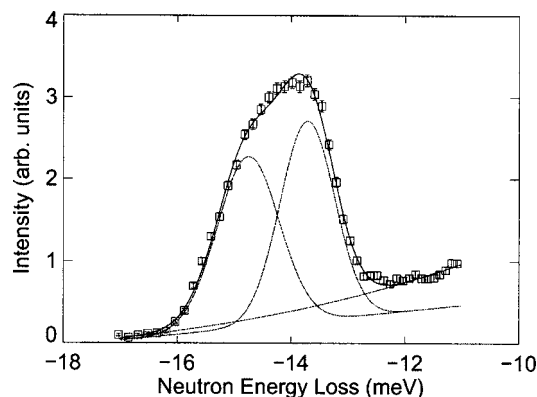


FIG. 6. Neutron energy gain peaks observed on DCS at 50 K fitted with three Gaussian components. Individual components are shown, and the solid line through the points is the overall fit to the data.

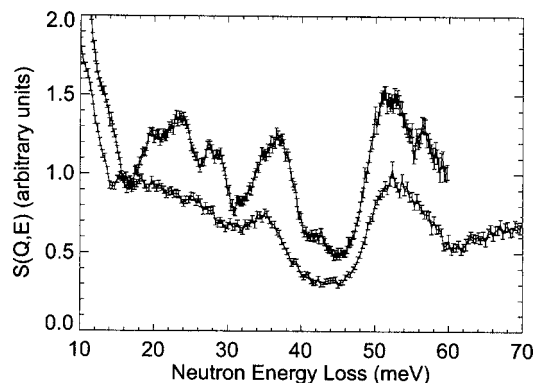


FIG. 7. Upper trace is $\text{H}_2/\text{THF}/\text{D}_2\text{O}$ measured at 8 K using an incident energy of 70 meV on Pharos. The lower curve is the equivalent spectrum measured for $\text{THF}/\text{D}_2\text{O}$ at 8 K using an incident energy of 120 meV. Both curves are a sum of $S(Q,E)$ for $Q=1-5 \text{ \AA}^{-1}$.

(3) one of the peaks fitted to the neutron energy loss spectrum is not a rotational transition. Option 2 is very unlikely in view of the small splitting of the $J=1$ state (0.6–1 meV), indicative of a small hindering potential and correspondingly small perturbation of the $J=2$ state, which is at 44.1 meV (i.e., a gap of 29.4 meV) for an unperturbed hydrogen molecule.

Assignment of the four peaks to states for two adsorption sites is challenging. Fortunately the temperature dependence is helpful in this respect. At 5 K, kT is approximately 0.5 meV and this increases to approximately 5 meV at 50 K. As the 15.22 meV is only marginally populated at 5 K, the separation between the states must be closer to 2.5–3 times 0.5 meV. This argues for a combination of the 12.83 and 15.22 meV states to be two of the split $J=1$ states for one site. This would make the 12.83 meV state the favored one at 5 K. However, there is little intensity at 12.83 meV in the spectrum taken at 5 K (Fig. 4). This argues in favor of a 13.86 meV lowest energy state derived from the free molecule $J=1$ state (option 3).

This implies that there is a single hydrogen adsorption site with a split $J=1$ triplet at 13.87, 14.57, and 15.22 meV (Table I). This is also consistent with the higher energy centroid for the neutron energy gain peak at 8 K measured on Pharos as compared to the DCS data taken at 5 K. A consequence of this assignment is that there should be excitations from the 15.22 meV state to the other two states in the triplet in neutron energy gain at 0.7 and 1.35 meV. Careful examination suggests that there may be extra intensity in that region of the spectrum, but there is significant intensity from the host clathrate modes in that region and the intensity of these features is expected to be weak since they originate from orthohydrogen.

Unfortunately, it is not possible to determine which of these excitations represent transitions between rotational states as there is no equivalent feature expected to be present in neutron energy gain (i.e., all the molecules will be in the lowest lying $J=1$ or $J=0$ states at 8 K).

For the free hydrogen molecular rotor, the $J=2$ state is expected to lie 42.81 meV ($6B$) above the energy of the $J=0$ ground state. As the external potential is weak (small perturbation of the $J=1$ states), it is tempting to assign the

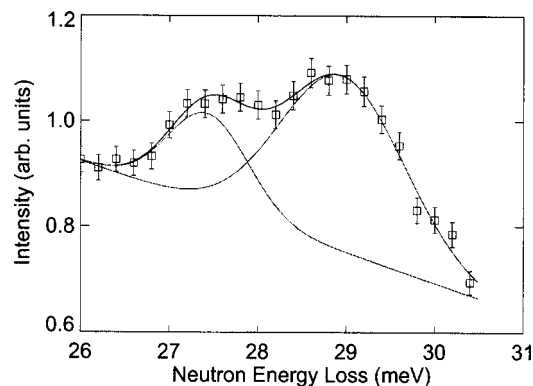


FIG. 8. Two Gaussians plus sloping background fit of the Pharos data measured at 8 K with 70 meV incident neutrons. Individual components are shown, and the solid line through the points is the overall fit to the data.

broad feature at approximately 37 meV to some of the $J=2$ states (five fold degeneracy in the free molecule). This would imply that the other features arise from translational quantum states of the confined molecule. It should also be noted that the hydrogen molecule can “ride” along with any collective excitation in the THF-ice lattice and thereby enhance the intensity of existing features present in the binary clathrate.

At the higher energies, there is considerable scattering in neutron energy loss between 20 and 60 meV. The interpretation of these features is that they represent many transitions to excited translational states of both ortho- and parahydrogen, in addition to a weakly split series of $J=0 \rightarrow 2$ transitions in the vicinity of 43 meV (expected to be weak⁹) and $J=1 \rightarrow 2$ around 28.5 meV. Indeed, there are two relatively sharp peaks at 27.44 and 28.95 meV (Fig. 8), and this doublet is therefore assigned to the $J=1 \rightarrow 2$ transitions. As expected, there is a feature in the vicinity of 42 meV which is interpreted as the weak $J=0 \rightarrow 2$ transition.

B. Analysis of translational quantum states

Neutron diffraction has shown that a single hydrogen molecule resides in the smaller 5^{12} cage in the THF-ice clathrate.³ There are two consequences of this confinement, the effect of an anisotropic external potential on the rotational quantum states and the imposition of constraints on the translational periodicity of the molecular wave function. From the analysis of the scattering data, the external potential causes only a small perturbation of the rotational quantum states. However, confinement on the scale of a few angstroms has dramatic consequences for the translational quantum states. This effect is explored using two simple solutions to the Schrödinger equation, namely, particle in a box and particle in a sphere, and also by comparison with a recently published quantum calculation for hydrogen in the specific environment of the 5^{12} cage in an ice clathrate.

1. Computational five-dimensional quantum theory

A recently published five-dimensional (5D) quantum theoretical treatment of hydrogen in the dodecahedral cage of SII ice clathrate¹⁰ provides detailed predictions for the rotational and translational quantum states of the hydrogen

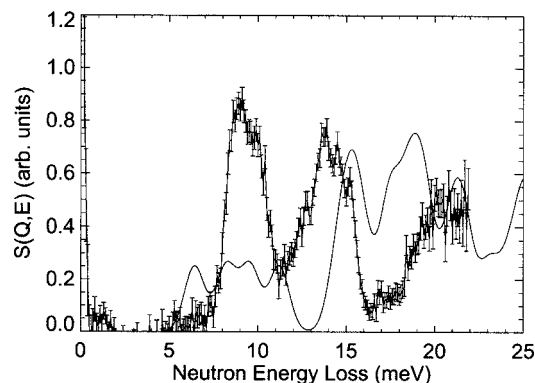


FIG. 9. Comparison between the prediction from the 5D quantum theoretical model (line) and the data measured on Pharos at 8 K.

molecule. These theoretical results are compared with the experimental results in Fig. 9, again assuming equal intensity for all of the transitions. The comparison is limited to a range up to approximately 28 meV. The band at 9 meV is reproduced, although the predicted transition at 6.4 meV is not observed. Another discrepancy is larger than observed splitting of the $J=1$ rotational quantum state, where theory predicts transitions at 11.22, 14.5, and 18.67 meV, while the interpretation of the experiment discussed above indicates that the transitions are at 13.87, 14.57, and 15.22 meV.

As the orthohydrogen ground state is not observed below 13.5 meV, the assignment of the first two transitions on the basis of a comparison between the energy loss and gain data is solid. However, the assignment of the 15.22 meV transition as the $(1,1)_u$ state [rotational (l,m) , symmetry ungerade; notation from Ref. 10] is not as certain, and it could arise from a transition to a translational quantum state. However, based on the 13.87–14.57 meV gap, we would expect the $(1,1)_u$ state to be roughly the same gap to the higher side of the 14.57 meV transition (i.e., 15.3 meV) as is the case in the theory result (−3.28 and +4.17 meV). The original assignment of the triplet about 14.57 meV to a split $J=1$ state is sound based on these arguments, and the predicted splitting is much larger than found experimentally, although they are both small on the scale of the rotational constant B .

Assignment of the two features at 8.77 and 10.01 meV is consistent with the expected gap between the $J=0$ (0,0,0) ground state and the excited (0,1,0) and (0,0,1) translational states (8.21 and 9.56 meV). However, there is no evidence for a separate (1,0,0) state around 6 meV. It is possible that the calculation overestimated the anisotropy of the translational states, and this is consistent with the uneven intensity distribution in these two peaks. It is quite likely that the transition to the third translational state is not resolved from the other two transitions.

On the neutron energy gain side, the broad distribution centered about 5 meV has not been discussed. It cannot arise from a rotational tunneling transition, as it is not present in neutron energy gain, and the sample temperature of 8 K requires that it should be associated with an excited state that cannot transition to the ground state. This then requires that the transition be associated with the $J=1$ states, and they represent transitions from orthohydrogen to the excited trans-

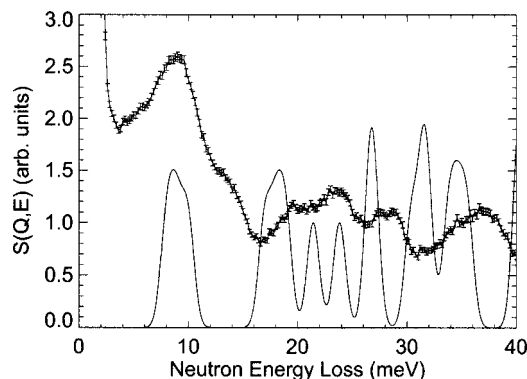


FIG. 10. Comparison between prediction of particle in a box model (line) and the experimental data measured at 8 K on Pharos.

lational ground states of parahydrogen. The gap between the parahydrogen excited translational states (8.76 and 9.99 meV) and the $J=1$ states populated at 8 K (mainly 13.87 and 14.57 meV) is approximately 4.6 meV.

Although the sophisticated computational approach is attractive, it is not straightforward to determine why there is significant disagreement between experiment and theory. The next sections will discuss the application of three very simple models for the translational quantum states of the confined hydrogen molecules. Although simple, they provide semi-quantitative insight into the interaction between the clathrate framework and the adsorbed hydrogen

2. Particle in a box

The simplest approach to understanding the translational quantum states is to consider the hydrogen to be in a cage that approximates to a three-dimensional rectangular box with infinitely high confinement potential. This is not expected to be quite correct, as there are openings in the cage and the shape is a crude approximation. The solution to the Schrödinger equation is¹¹

$$E_{n_1, n_2, n_3} = \frac{h^2}{8m} \left(\left(\frac{n_1}{L_1} \right)^2 + \left(\frac{n_2}{L_2} \right)^2 + \left(\frac{n_3}{L_3} \right)^2 \right), \quad n_i = 1, 2, 3, \dots,$$

where $L_{1,2,3}$ are the lengths of the sides and m is the mass of the hydrogen molecule.

From the preliminary analysis we know that the peak at approximately 9 meV is associated with the center-of-mass motion of the hydrogen. This peak contains at least two features, centered at 8.7 and 9.6 meV. The relative areas of the two Gaussians fitted to this feature are similar, with the latter approximately twice the width of the former. This suggests that there are really three features in this band, corresponding to different values for L_i . A reasonable reproduction of this feature using the particle in a box equation for the separation between the ground state ($n_{i,j,k}=1$) and the first excited states ($n_{i,j}=1, n_k=2$), using lengths of 1.75, 1.85, and 1.95 Å.

A qualitative comparison between this model and the measured spectrum is shown in Fig. 10, where the expected transitions are plotted as a series of Gaussian peaks together with the experimental data. Although it is possible to reproduce an excitation at approximately 9 meV using reasonable lengths for the size of the box, there are many predicted

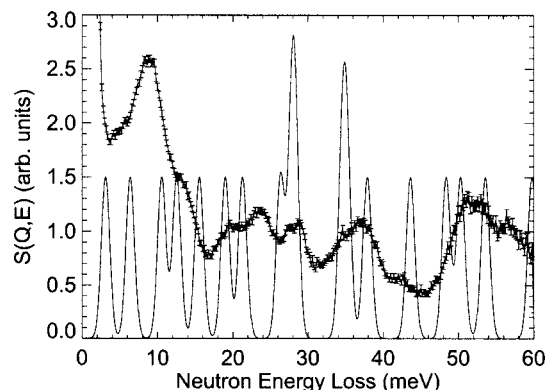


FIG. 11. Comparison between prediction for particle in a sphere of radius of 1.8 Å (line) and the data taken on Pharos at 8 K.

transitions at higher energies that are not present in the data. Some of these transitions could be shifted by rotation-translation coupling, but the sophisticated computational study described in Sec. I (Ref. 10) predicts that this effect is on the order of a few percent.

3. Particle in a sphere

A spherical shape of the cavity is likely to be a much better approximation to the 5^{12} cavity. The solution to the Schrödinger equation for this model is¹²

$$E_l = \frac{u_{l,k}^2 \hbar^2}{2mr^2},$$

where k represents the series of points where the spherical Bessel functions of order l cross zero, m is the mass of the hydrogen molecule, and r is the radius of the sphere.

Two of the predicted states are close in energy, and the radius of the cavity is chosen so that the energy gap between them approximately matches the location of the excitations at 8.76 and 9.99 meV. A comparison between this model and the experimental spectrum is shown in Fig. 11. There is no better agreement than the case for the particle in the box model. There are still too many predicted transitions, e.g., no peaks at 3.1 and 6.4 meV in the experimental data and no sign of the predicted peak at approximately 15.6 meV.

4. Particle on the surface of a sphere

The implicit assumption in both of the above analytical models is that there is no potential within the dodecahedral cage that favors particular regions of the available space. This is unlikely to be the case, and *ab initio* calculations by Patchkovskii and Tse at the MP2 level predicted a potential well approximately 1.1 Å from the center of the cage. As the potential difference between the center and this well is relatively large at 50 meV, the hydrogen molecular wave function will be localized by this barrier.

This effect can be roughly approximated using the analytical solution for a particle constrained to be on the surface of a sphere. The energy levels for this model are given by¹¹

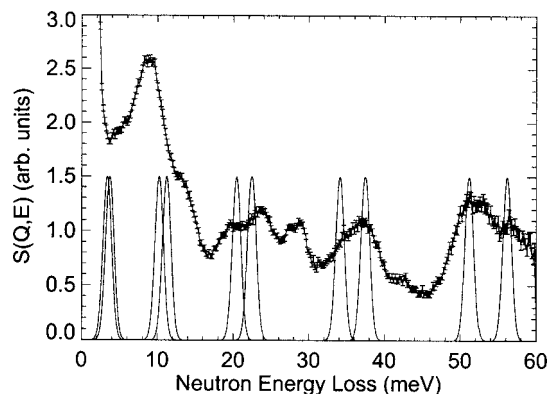


FIG. 12. Comparison between the excitations expected for particle on the surface of a sphere with radii of 1.05 and 1.1 Å, and the data taken on Pharos at 8 K.

$$E_l = \frac{l(l+1)\hbar^2}{2mr^2}, \quad l = 0, 1, 2, \dots,$$

where m is the mass of the hydrogen molecule and r is the radius of the sphere. A comparison between the data from Pharos and this model is shown in Fig. 12. As there are at least two peaks at approximately 9 meV, the figure shows two series of peaks for sphere radii of 1.05 and 1.1 Å. The origin of the splitting is likely due to the removal of the degeneracy of the states as the cavity is not exactly spherical.

There is reasonably good agreement, particularly as there are far fewer excitations predicted than is the case for the other models. All of the peaks are accounted for as the bands at 14, 28, and 42 meV arise from transitions between rotational quantum states. There is a predicted transition at approximately 3.5 meV, but this could be obscured by the significant scattering from the THF-ice clathrate at those lower energies.

5. Summary of comparisons for translational quantum states

It is clear from the discussion that neither simple models nor sophisticated computational quantum theory correctly predicts all of the translational quantum transitions for hydrogen in the 5^{12} cage of THF-ice clathrate. The 5D theory, particle in a box, and particle in a sphere model all predict many more transitions than are observed. Confinement of the hydrogen onto the surface of a sphere gives more promising results, with the assumption that the apparent peak splittings arise from a splitting of degenerate states.

C. Temperature dependence

As the temperature of the sample is increased from 8 K, there will be temperatures at which the THF and hydrogen molecules will exhibit diffusive motion on the length and time scales of the neutron experiments. As the DCS instrument was operated with a moderately high elastic energy resolution of approximately $90 \mu\text{eV}$ (full width at half maximum), this diffusive motion would have to occur on the picosecond time scale in order to be observed. It is expected that the onset of diffusive motion will occur at different characteristic temperatures for the THF and the hydrogen.

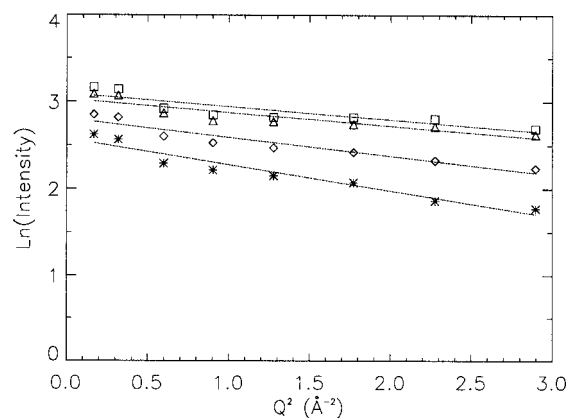


FIG. 13. Debye-Waller plots from the DCS data, with the intensity summed over the neutron energy loss range of ± 1 meV.

From the measurements made on the THF-ice binary clathrate, quasielastic scattering is observed at 50 K and above. As the THF is fully deuterated, this scattering is coherent, and the intensity and width of the scattering are very dependent on the momentum transfer. As the hydrogen is known to occupy the small cage while the THF is in the larger cage, it is likely that the scattering from the THF-ice clathrate will not be significantly affected by the presence of the hydrogen. This is consistent with the excellent match between the inelastic scatterings from the clathrate with and without hydrogen below 7 meV. If this assumption holds, then the THF-ice scattering data can be subtracted from the $\text{H}_2/\text{THF}/\text{D}_2\text{O}$ data to obtain the scattering from the hydrogen only.

This subtraction was carried out and the results are inspected for any sign of a quasielastic broadening over the range of 5–150 K. There was no evidence of diffusive broadening or any sign of a shape anomaly in the vicinity of the elastic scattering indicative of a problem arising from the subtraction of the THF/ice background scattering. The conclusion is that the hydrogen molecule does not exhibit any diffusive motion on the length and time scales of the experiment up to a temperature of 150 K. This is consistent with the requirement that the sample be close to the melting point of the clathrate to incorporate the hydrogen into the structure.

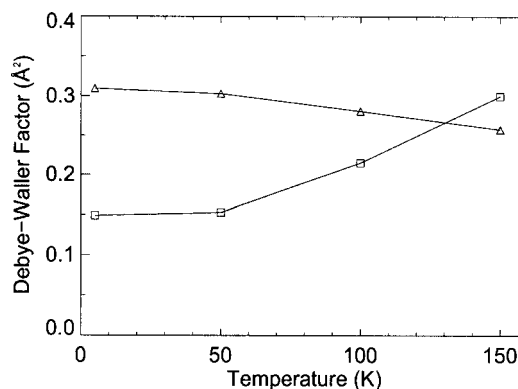


FIG. 14. Temperature dependence of the hydrogen molecule Debye-Waller Factor (squares). Also shown is the variation in the zero- Q intercept of the fits in Fig. 13 (triangles, arbitrary units).

TABLE I. Results from fitting the H₂ scattering data measured at 8 K. Estimated 1 σ errors are given in parentheses. The resolution estimates are from a Monte Carlo simulation of the Pharos instrument as described in the text. The assignments are indicated as rotational (*R*) or translational (*T*) modes of the hydrogen molecule. The feature at 12.83 is broad and potentially an artifact of the fitting.

Neutron energy	Assignment	Position (meV)	Intensity (arb. units)	FWHM (meV)	Resolution (meV)
Gain $\chi^2=0.74$	<i>R</i> , <i>J</i> =1 \rightarrow 0	-15.33 (0.36)	0.031 (0.015)	1.45 (0.32)	2.04
	<i>R</i> , <i>J</i> =1 \rightarrow 0	-14.19 (0.11)	0.108 (0.011)	1.52 (0.12)	2.00
	Phonons	-4.58 (0.07)	0.071 (0.003)	2.95 (0.15)	1.64
Loss $\chi^2=0.86$	<i>T</i>	8.76 (0.07)	0.77 (0.06)	1.28 (0.08)	1.15
	<i>T</i>	9.99 (0.09)	0.60 (0.05)	1.36 (0.19)	1.04
	<i>T?</i>	12.83 (0.40)	0.36 (0.05)	2.33 (0.67)	1.00
	<i>R</i> , <i>J</i> =0 \rightarrow 1	13.87 (0.05)	0.45 (0.18)	1.00 (0.25)	0.96
	<i>R</i> , <i>J</i> =0 \rightarrow 1	14.57 (0.03)	0.35 (0.08)	0.50 (0.09)	0.93
	<i>R</i> , <i>J</i> =0 \rightarrow 1	15.22 (0.04)	0.45 (0.03)	0.72 (0.08)	0.91

The intensity of the elastic scattering from the hydrogen will have a Q dependence that follows the Debye-Waller factor. The analysis is subject to interference from Bragg scattering from the clathrate, and the DCS data were analyzed with all detectors showing Bragg scattering removed. The signal integrated between -1 and 1 meV as a function of momentum transfer is plotted in Debye-Waller form in Fig. 13, including linear fits to extract the mean square displacements ($\langle u^2 \rangle$). Increasing the temperature should increase $\langle u^2 \rangle$, and the onset of a transition is often signaled by a rapid increase in $\langle u^2 \rangle$. There is a slow increase above 50 K, which is consistent with the lack of any quasielastic scattering. However, the zero momentum transfer intercept should remain constant as a function of temperature, and this is not the case as is also shown in Fig. 14. This suggests that there may be some coupling between the motion of the hydrogen and the THF molecules, resulting in this unexpected drop in the zero- Q intercept.

V. CONCLUSION

Hydrogen was successfully loaded into a deuterated THF-water ice clathrate and measured on the Pharos and DCS inelastic neutron scattering spectrometers with similar results. The rotational quantum states are mildly perturbed from their free molecule energies, demonstrating that the potential experienced by the hydrogen adsorbed in the dodecahedral 5¹² cage is weakly anisotropic. A series of transitions between translational quantum states are also observed.

A computational quantum chemical study of hydrogen in the 5¹² cage of structure-II ice clathrate¹⁰ predicts a larger shift in the rotational transitions and many more transitions between translational states than is observed. Comparisons between three simple exact solutions to the Schrödinger equation suggest that the most appropriate model confines the hydrogen molecule into a spherical shell approximately 1.05–1.1 Å from the cage center. This result is in good agreement with quantum chemical calculations for the hydrogen translational potential in this cage.¹³ The observed

bands with more than one peak are interpreted to arise from a lifting of the degeneracy as the shell is not exactly spherical.

No quasielastic scattering is observed for the hydrogen up to a temperature of 150 K. However, there is a distinct increase in the Debye-Waller factor between 100 and 150 K, indicative of the onset of motion with an increased amplitude.

ACKNOWLEDGMENTS

The authors thank Timothy Jenkins for his help which enabled the experiment at NIST. This work has benefited from the use of the Lujan Neutron Scattering Center at LANL-SCE, which is funded by the Department of Energy's Office of Basic Energy Sciences. Los Alamos National Laboratory is operated by Los Alamos National Security LLC under DOE Contract No. DE-AC52-06NA25396. This work utilized facilities supported in part by the National Science Foundation under Agreement No. DMR-0454672.

¹W. L. Mao, H. K. Mao, A. F. Goncharov, V. V. Struzhkin, Q. Z. Guo, J. Z. Hu, J. F. Shu, R. J. Hemley, M. Somayazulu, and Y. S. Zhao, *Science* **297**, 2247 (2002).

²L. J. Florusse, C. J. Peters, J. Schoonman, K. C. Hester, C. A. Koh, S. F. Dec, K. N. Marsh, and E. D. Sloan, *Science* **306**, 469 (2004).

³K. C. Hester, T. A. Strobel, E. D. Sloan, C. A. Koh, A. Huq, and A. J. Schultz, *J. Phys. Chem. B* **110**, 14024 (2006).

⁴A. P. Smith, R. Benedek, F. R. Trouw, M. Minkoff, and L. H. Yang, *Phys. Rev. B* **53**, 10187 (1996).

⁵C. N. Tam, F. R. Trouw, and L. E. Iton, *J. Phys. Chem. A* **108**, 4737 (2004).

⁶S. A. FitzGerald, T. Yildirim, L. J. Santodonato, D. A. Neumann, J. R. D. Copley, J. J. Rush, and F. Trouw, *Phys. Rev. B* **60**, 6439 (1999).

⁷J. R. D. Copley and J. C. Cook, *Chem. Phys.* **292**, 477 (2003).

⁸K. Lefmann and K. Nielsen, *Neutron News* **10**, 20 (1999); P. Willendrup, E. Farhi, and K. Lefmann, *Physica B* **350**, 735 (2004).

⁹J. A. Young and J. U. Koppel, *Phys. Rev.* **135**, A603 (1964).

¹⁰M. Xu, Y. S. Elmatad, F. Sebastianelli, J. W. Moskowitz, and Z. Bacic, *J. Phys. Chem. B* **110**, 24806 (2006).

¹¹P. W. Atkins, *Molecular Quantum Mechanics* (Clarendon, Oxford, 1970).

¹²D. J. Griffiths, *Introduction to Quantum Mechanics* (Prentice Hall, New Jersey, 1995).

¹³S. Patchkovskii and J. S. Tse, *Proc. Natl. Acad. Sci. U.S.A.* **100**, 14645 (2003).